Acta Materialia 214 (2021) 116993

Contents lists available at ScienceDirect

Acta Materialia

journal homepage: www.elsevier.com/locate/actamat

Full length article

# Atomic diffusivities in amorphous and liquid Cu-Zr: Kirkendall effects and dependence on packing density

S.V. Ketov[a,1], Yu.P. Ivanov[b,c,1], B. Putz[a,2], Z. Zhang[a,d], J. Eckert[a,d,3], A.L. Greer[b,e,*]

[a] Erich Schmid Institute of Materials Science, Austrian Academy of Sciences, Jahnstraße 12, Leoben A-8700, Austria
[b] Department of Materials Science & Metallurgy, University of Cambridge, Cambridge CB3 0FS, United Kingdom
[c] School of Natural Sciences, Far Eastern Federal University, Vladivostok 690950, Russian Federation
[d] Department of Materials Science, Chair of Materials Physics, Montanuniversität Leoben, Jahnstraße 12, Leoben A-8700, Austria
[e] WPI Advanced Institute for Materials Research, Tohoku University, Sendai 980-8577, Japan

ARTICLE INFO

*Article history:*
Received 1 February 2021
Revised 7 May 2021
Accepted 10 May 2021
Available online 19 May 2021

*Keywords:*
Amorphous alloy
*In-situ* transmission electron microscopy (TEM)
Interdiffusion
Kirkendall effect
Multilayer thin films

ABSTRACT

A novel method for measurement of atomic interdiffusivity is applied to amorphous Cu-Zr close to its glass-transition temperature $T_g$. Sputter-deposited multilayers are examined in cross-section by transmission electron microscopy and energy-dispersive X-ray spectroscopy. Mapping the evolution of composition profiles gives the interdiffusivity, which is orders of magnitude higher than if coupled to the viscosity expected near $T_g$. Kirkendall drift of interlayer interfaces in both amorphous and supercooled liquid states (i.e. below and above $T_g$), and associated voiding in the liquid, show that the diffusivity of copper greatly exceeds that of zirconium. Amorphous Cu-Zr is known to show maxima in atomic packing density at sharply defined compositions. The comparison of the two compositions in the present work provides the first direct evidence that denser packing is associated with lower atomic interdiffusivity. The lower interdiffusivity is governed by a lower diffusivity of copper, and reflects a lessened degree of decoupling of the copper (fast) and zirconium (slow) diffusivities in an efficiently packed glass. The new insights help to understand issues ranging from glass-forming ability to the controlled generation of nanovoided structures.



## 1. Introduction

Alloys of late transition metals (LTM – Co, Cu, Fe, Ni) with early transition metals (ETM – Hf, Nb, Ti, Zr) are the bases of many bulk metallic glasses (BMGs). In such glasses, the LTM atoms are smaller and have diffusivities much higher than the ETM atoms [1–3]. The soft LTM-ETM interatomic potentials favour fast diffusion of the LTM and glass formation [4]. The intrinsically asymmetric interdiffusion in such glasses underlies solid-state amorphization [2], and can give void formation enabling fabrication of amorphous-alloy nanospheres and nanotubes [5,6], examples of the exploitation of the Kirkendall effect [7]. The internal stresses arising from asymmetric interdiffusion in LTM-ETM amorphous alloys have been used in optimizing magnetic properties [8].

Atomic diffusion in amorphous LTM-ETM systems has been widely studied by conventional tracer methods [3]. Interdiffusion, however, has mostly been studied in multilayered, i.e. compositionally modulated, thin films made by physical vapour deposition [2,9]. In these studies, the period $\Lambda$ of the modulation was small (1–10 nm) in order that the decay of the modulation could be measured from the decay of X-ray satellite reflections. Extensive studies of amorphous Ni-Zr multilayers [9,10] included finite-element modelling of the composition profiles during interdiffusion. This modelling showed effects of the diffusional asymmetry, but the inferred Kirkendall drift of the Matano interface between the layers was not directly observed.

The Cu-Zr system is amongst the most studied binary glass-forming systems, yet has not been subject to any measurements of interdiffusion. It is of interest to correlate atomic diffusivities with changes in packing density that can be strongly dependent on composition [11]. We work on multilayers of larger $\Lambda$ (~130 nm) in order that the shapes of the composition profiles can be reli-

* Corresponding author at: Department of Materials Science & Metallurgy, University of Cambridge, Cambridge CB3 0FS, United Kingdom.
*E-mail address:* alg13@cam.ac.uk (A.L. Greer).
[1] These authors contributed equally to this work.
[2] Present address: EMPA Swiss Federal Laboratories for Materials Science and Technology, Feuerwerkerstraße 39, CH-3602 Thun, Switzerland
[3] Adjunct with National University of Science and Technology «MISiS», Leninsky Prosp., 4, 119049, Moscow, Russia

https://doi.org/10.1016/j.actamat.2021.116993

ably characterized by analytical transmission electron microscopy (TEM). From such profiles, we can better understand the diffusion mechanism, and can directly measure the Kirkendall drift velocity as homogenization proceeds.

Voiding has been reported in homogenizing amorphous Ge-Si multilayers [12], but not so far in amorphous alloy multilayers. Voiding in multilayers is of interest for the controlled development of nanoscale porosity to enhance thin-film functionality in a range of applications [13].

## 2. Experimental methods

### 2.1. Deposition

The sequences of layers were deposited, without breaking vacuum, in a custom-built direct-current (dc) magnetron-sputtering system. For each sample, first a tantalum base-layer was deposited to ensure isolation of the amorphous Cu-Zr from the substrate, and then a five-period multilayer of Cu-rich and Zr-rich layers. Two sets of samples were deposited, with and without a top capping layer of tantalum. The presence, or not, of the capping layer is not significant for the behaviour within the Cu-Zr multilayers (§3.2). The two sets of samples have overall compositions (at.%, measured by energy-dispersive X-ray spectroscopy, EDX) of $Cu_{56}Zr_{44}$ and $Cu_{59}Zr_{41}$, henceforth referred to as 56 Cu and 59 Cu.

The substrates, 10 × 10 $mm^2$ silicon (100) wafers with native oxide, were ultrasonically cleaned in ethanol for 5 min, and placed on a rotatable table 40 mm from the targets. The targets were Ta (99.97% purity), Cu (99.97% purity) and Zr (99.99% purity) plates (Kurt J. Lesker Co.) mounted on three unbalanced AJAA320-XP magnetrons, aligned in a confocal arrangement. The base pressure of the chamber before each deposition run was below 1 × $10^{-5}$ Pa. Prior to film deposition, the targets were pre-sputtered with closed shutters for 1 min. The sputtering gas was argon, maintained at 0.5 Pa, with a continuous flow rate of 40 sccm. The dc sputtering was in power-controlled mode. For deposition of tantalum the power was 138 W. The Cu-Zr layers were deposited by co-sputtering from the elemental targets. The composition was controlled by adjusting the power applied to the targets: Cu-rich layers with Cu at 70 W and Zr at 130 W, for 36 s/layer (88 nm/min); Zr-rich layers with Cu at 30 W and Zr at 170 W, for 64 s/layer (75 nm/min). The measured layer thicknesses and compositions (and $T_g$ values [14]) are given in Table 1. After deposition of each layer, co-deposition was stopped to adjust the power values for deposition of the next layer and to achieve a sharp boundary between the layers.

Interpolating between measured values for Cu-Zr [14], we estimate that for 56Cu $T_g$ = 687 K, and for 59Cu $T_g$ = 706 K.

### 2.2. Annealing

Samples on their substrates, wrapped in titanium foil, were placed in a vacuum furnace (Xerion Xtube) that was evacuated to <5 × $10^{-5}$ Pa, heated to the chosen annealing temperature 673±5 K, and cooled. As the heating and cooling rates were relatively low (10 K $min^{-1}$ and 3–4 K $min^{-1}$ respectively), it was necessary to account for annealing effects during the heating and cooling. Based on measured temperature-time profiles, corrections to the nominal annealing times were computed, assuming that the diffusivities have an Arrhenius temperature dependence. From collected data for the tracer diffusivities of (Co,Ni) in amorphous (Co or Ni)-Zr [2,9], we estimate an activation energy of 131(±20%) kJ $mol^{-1}$. Using this value, the overall effective annealing times were 23±2 min and 43±2 min.

### 2.3. TEM

Each specimen was transferred from the multilayer sample (as-deposited, or after an ex-situ anneal) to a standard TEM grid. For in-situ heating, a specimen was transferred from the as-deposited 56Cu multilayer to a windowed point on a chip (DENSsolutions). The procedures for specimen preparation and for TEM examination were as used by Ivanov et al. [15]. The compositional analysis (Cliff-Lorimer method) based on EDX spectra gives absolute elemental contents with accuracy better than 0.5 at.%. With the probe diameter of ~0.2 nm, the spatial resolution is limited by the step size during spectrum acquisition, namely 0.5 nm. At the length-scales in our work, the measured composition profiles are not significantly distorted by this resolution limit. In addition, TEM was performed at 300 kV on a JEOL ARM300F double-corrected microscope equipped with Gatan OneView Camera (4k × 4k pixels). In this case, the sample was flash-heated in-situ into the supercooled liquid state.

## 3. Results

### 3.1. Structure of the samples

High-angle annular dark-field (HAADF) images (Fig. 1) show full cross-sections of the 56Cu and 59Cu samples, with the electron beam accurately parallel to the interfaces between the layers. The lighter and darker grey stripes are the Cu-Zr multilayers. Apart from the compositional layering, the as-deposited and annealed samples are uniform. The images and SAED patterns (insets) show that the Cu-Zr multilayers are fully amorphous upon deposition and remain so after annealing. In these dark-field images, the lighter areas are those with higher density. The contrast between the Cu-rich (lighter) and Zr-rich (darker) layers decreases on annealing. This homogenization proceeds faster in 59Cu.

### 3.2. Evolution of the composition profiles

The energy-dispersive X-ray spectroscopy (EDX) mapping (Fig. 2) qualitatively confirms the interdiffusion inferred from Fig. 1. On annealing the thicknesses of the Cu-rich and Zr-rich layers change, within a multilayer period Λ that stays constant. These effects can be quantified from EDX line profiles (Fig. 3). On these, the five Cu-rich layers are labelled ① (next to the Ta base layer) to ⑤ (just underneath the top Zr-rich layer) to facilitate discussion.

The 59Cu sample has no tantalum capping layer. On annealing, the top Zr-rich layer becomes richer in Zr and poorer in Cu (Fig. 3e and f), interpreted to represent the formation of a Zr-rich oxide. After the 23-min anneal, a Cu-rich shoulder has developed on the upper (right-hand in Fig. 3e) side of layer ⑤. The formation of such a buried layer enriched in the more noble metal is common in

**Table 1**
Characteristics of the as-deposited compositionally modulated films.

| Sample code | Cu-rich layers | | Zr-rich layers | | Overall | Capping layer |
|---|---|---|---|---|---|---|
| | *d* (nm) | at.% Cu | *d* (nm) | at.% Cu | at.% Cu | |
| 56Cu | 53 | 72 | 80 | 45 | 56 | yes |
| 59Cu | 52 | 75 | 78 | 49 | 59 | no |

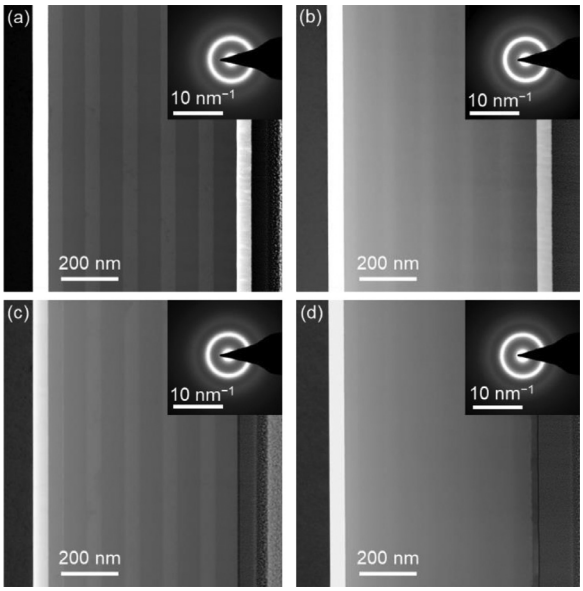


**Fig. 1.** Cross-sectional TEM (HAADF) images and corresponding SAED patterns (insets) for amorphous Cu-Zr multilayers: for the 56Cu sample, (a) as-deposited and (b) annealed; and for the 59Cu sample, (c) as-deposited and (d) annealed. The anneal was at 673 K for 43 min. The substrate is on the left. On top of that (i.e. to the right) in succession are a tantalum base layer (white), a five-period multilayer (the thicker, darker layers are Zr-rich), a tantalum capping layer (white) for (a,b) only, and finally the platinum layer deposited in the thin-foil preparation.

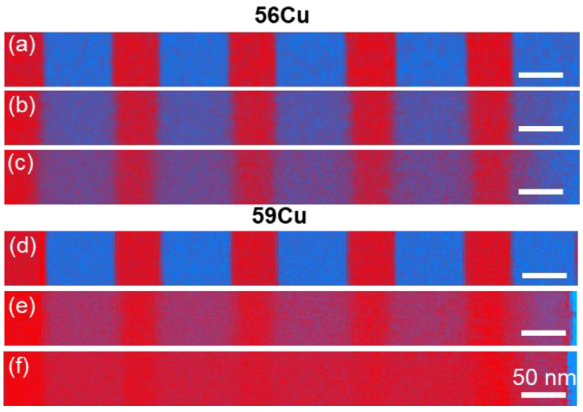


**Fig. 2.** EDX mapping of the five-period multilayer in the 56Cu and 59Cu cross-sections in Fig. 1: (a,d) as-deposited, (b,e) annealed at 673 K for 23 min, (c,f) annealed at 673 K for 43 min. On annealing, there is interdiffusion: the Cu-rich layers (red) get thinner, the Zr-rich layers (blue) get thicker. (For interpretation of the references to colour in this figure legend, the reader is referred to the web version of this article.)

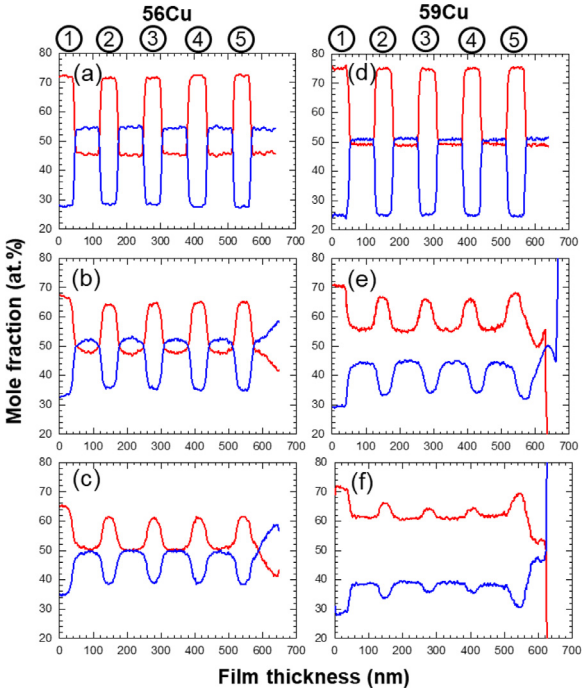


**Fig. 3.** EDX line profiles through the six multilayers in Fig. 2, showing the Cu content (red lines) and Zr content (blue lines): (a,d) as-deposited; (b,e) annealed at 673 K for 23 min; (c,f) annealed at 673 K for 43 min. (For interpretation of the references to colour in this figure legend, the reader is referred to the web version of this article.)

selective oxidation, and has been characterized for oxidation of a Cu-Zr-Al MG [16]. The 56Cu sample (with tantalum capping layer) shows no equivalent development of a Cu-rich shoulder; rather the top Zr-rich layer loses copper into the capping layer (Fig. 3b and c). Copper and tantalum are immiscible, but copper can diffuse fast along grain boundaries in tantalum, making its way to the outer surface. The effective diffusivity must depend on grain size. Extrapolated to 673 K, the effective $D_{Cu}$ in a deposited tantalum layer [17] would be of order $3 \times 10^{-13}$ m$^2$ s$^{-1}$, orders of magnitude higher than the diffusivity of copper in amorphous Cu-Zr (§3.4).

In 56Cu and 59Cu, there is no similar depletion of copper from layer ① in contact with the tantalum base layer, which is effectively inert as there is no sink for copper on the other side (i.e. the substrate). In both samples on annealing, the copper content of layers ②, ③ and ④ decreases as these layers lose copper by diffusion into the Zr-rich layers on each side. The copper content of layer ① does not decrease so much, losing copper only on one side. In the 56Cu sample, layer ⑤ shows a decay in copper content very similar to that in layers ②, ③ and ④ (Fig. 3b and c), because it also loses copper into the Zr-rich amorphous alloy on each side. In contrast, in the 59Cu sample, layer ⑤ loses less copper on annealing than do layers ②, ③ and ④ (Fig. 3e and f): the oxidized Zr-rich layer on top of layer ⑤ becomes effectively inert, and the behaviour in layer ⑤ is then similar to that in layer ①.

With or without a tantalum capping layer, layers ②, ③ and ④ evolve in a way that suggests little or no effect of the substrate or the top surface and no effect of oxidation.

### 3.3. Cu-Zr interdiffusion

The initial composition profiles are nearly square-wave (Fig. 3a and d). The interdiffusion would be symmetrical if $v_{Cu}D_{Cu} = v_{Zr}D_{Zr}$, where $D_{Cu}$ and $D_{Zr}$ are the chemical diffusivities of the two species, and $v_{Cu}$ and $v_{Zr}$ are the corresponding volumes per atom. In that case, interdiffusion would imply no net transport of volume across the interface between two layers. In an ideal case $D_{Cu}$ and $D_{Zr}$ would be independent of the alloy composition (over the range of the composition modulation), and the square-wave profile would evolve towards sinusoidal on annealing. The profiles do show some rounding, but retain square-wave character. The Cu-rich layers become thinner on annealing; this drift of the interlayer interfaces is the Kirkendall effect due to asymmetric interdiffusion, in which $v_{Cu}D_{Cu} > v_{Zr}D_{Zr}$. Assuming that the volume per atom scales with the cube of the Goldschmidt radii of the elements, $v_{Zr} \approx 1.95v_{Cu}$, so the drift shows that $D_{Cu} \gg D_{Zr}$, as expected (§1).

Modelling of interdiffusion in amorphous Ni-Zr multilayers [9,10] showed that, at least in quasi-steady state, a square-wave composition profile is maintained as the modulation amplitude decays on annealing. In that case, the usual analytical forms of the profile at an interface do not apply. Even though the square-wave

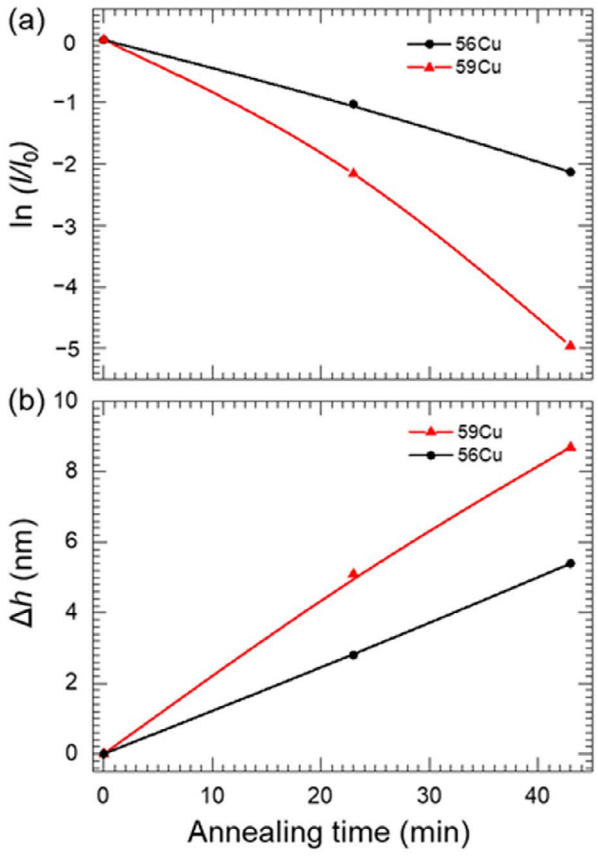


**Fig. 4.** Interdiffusion at 673 K in amorphous Cu-Zr multilayers characterized using changes in composition profiles measured using EDX mapping. (a) The decay of the composition modulation represented in terms of the relative intensity $I/I_0$ of first-order diffraction calculated from the first Fourier component of the modulation. (b) Kirkendall drift: the distance moved by an interface between Cu-rich and Zr-rich layers, estimated from the decrease in thickness of the Cu-rich layers.

character is not so fully retained in the present case, there is a similar problem of how to extract a value for the interdiffusivity $\tilde{D}$ from the composition profiles. This problem is worsened by dependence of $\tilde{D}$ on composition.

In analysis of interdiffusion in multilayers, the decay of the composition modulation was measured from the intensity of first-order X-ray satellite reflections [18]. This method gives relative values of the first Fourier component of the modulation, and the decay of that component is related simply to an overall $\tilde{D}$ [19,20]. The decay of the intensity $I$ of a first-order satellite relative to its initial value $I_0$ is given by [18]:

$$\frac{\partial \ln(I/I_0)}{\partial t} = \frac{-8\pi^2\tilde{D}}{\Lambda^2} \quad (1)$$

We simulate this method by evaluating the Fourier components of the composition profiles. Only two central periods are analysed, as these are not affected by substrate or surface effects (§3.2). The intensity of a first-order satellite is proportional to the square of the first Fourier component. The intensity decays (Fig. 4a) calculated from the measured composition profiles (Fig. 3) for 56Cu and 59Cu can be compared with those in the same format in the literature on interdiffusion in compositionally modulated thin films of metallic alloys, both amorphous and crystalline [19–21]. In plots of $\ln(I/I_0)$ vs time, $\tilde{D}$ is proportional to the gradient: a straight line would indicate a constant $\tilde{D}$.

In earlier work, mostly focused on measuring interdiffusivities at temperatures well below those for conventional diffusion measurements, the plots of $\ln(I/I_0)$ vs time show a rapid initial decay followed by a constant gradient at longer times. The constant gradient is used to extract the value of $\tilde{D}$, while the initial transient is attributed to the effects of structural relaxation [22] or the build-up of stresses [9]. In contrast, Fig. 4a shows decays that are near-linear; the curvature may reflect a breakdown in the diffusional analysis in the later stages of homogenization. In the earlier stages, taking the gradients of the lines linking the origin in Fig. 4a to the first data points at 23 min and applying Eq. (1), we obtain: $\tilde{D} = 1.7 \times 10^{-19}$ m$^2$ s$^{-1}$ for 56Cu, and $\tilde{D} = 3.4 \times 10^{-19}$ m$^2$ s$^{-1}$ for 59Cu.

We estimated the uncertainty in these $\tilde{D}$ values by also fitting the interdiffusion profiles to an error-function solution, and by comparing the values of $D_{Cu}$ derived from $\tilde{D}$ and from the interface drift velocity (§3.4). Overall, the uncertainty in $\tilde{D}$ arising from the difficulty of fitting non-ideal composition profiles is ±45%. This uncertainty in absolute values does not, however, affect the precision of the values for comparing 56Cu and 59Cu. The two compositions are treated identically and, in this 'side-by-side' study, the large difference in the effective interdiffusivities is immediately clear (Figs 1–3), even without any analysis of the profiles.

### 3.4. Interface drift

An advantage of the multilayer geometry is that the thickness of layers can be measured and used to determine the extent of interface drift, without the use of inert markers. Measurements were made on layer ③ in each stack. The drift of each interface increases linearly with anneal time (Fig. 4b), in contrast to the expected proportionality with the square root of time. This contrast may be because the two sides of the layer are too close to behave independently, especially at longer time. Taking the behaviour to be linear up to 23 min, the interface drift velocity is $U = 2.0 \pm 0.2$ pm s$^{-1}$ for 56Cu, and $3.7 \pm 0.3$ pm s$^{-1}$ for the 59Cu sample.

From the profiles of mole fraction of copper $X_{Cu}$ as a function of distance $x$ normal to the substrate, the interfacial composition gradients $\partial X_{Cu}/\partial x$ can be determined. The magnitude of the gradients on either side of layer ③ at 23 min are $1.2 \times 10^7$ m$^{-1}$ for 56Cu, and $5.9 \times 10^6$ m$^{-1}$ for the 59Cu sample (Fig. 3b and e).

Having the values of $\tilde{D}$, $U$ and $\partial X_{Cu}/\partial x$ at $t = 23$ min, we use the Darken relations [23] to try to evaluate $D_{Cu}$ and $D_{Zr}$. In the original derivation [23], it was assumed that the partial volume per atom is the same for the two species; that does not apply in the present case. Differing volumes of the two species can be taken into account [24], and we consider the special case where $D_{Cu} >> D_{Zr}$, in effect where $D_{Zr}$ is negligible. The relevant relations can then be expressed as:

$$\tilde{D} = \frac{\nu_{Zr}}{\nu_m} X_{Zr} D_{Cu} \text{and} \quad (2)$$

$$U = \frac{\nu_{Cu}\nu_{Zr}}{\nu_m^2} D_{Cu} \frac{\partial X_{Cu}}{\partial x} \quad (3)$$

where $\nu_m$ is the average (weighted by mole fraction) of $\nu_{Cu}$ and $\nu_{Zr}$ for the alloy composition. If copper and zirconium had the same volume per atom (i.e. $\nu_{Cu} = \nu_{Zr} = \nu_m$), then the terms $(\nu_{Zr}/\nu_m)$ and $(\nu_{Cu}\nu_{Zr}/\nu_m^2)$ would be 1, and Eqs. (2) and (3) simplify to more familiar forms. Since $\nu_m$ is composition-dependent, there are different values of $(\nu_{Zr}/\nu_m)$, 1.375 and 1.403, and of $(\nu_{Cu}\nu_{Zr}/\nu_m^2)$, 0.97 and 0.99, for 56Cu and 59Cu. Thus, at least for Eq. (2), it is important to take account of the difference between $\nu_{Cu}$ and $\nu_{Zr}$.

Using Eqs. (2) and (3), we have two independent means to calculate $D_{Cu}$ (Table 2). Given the approximations and assumptions, the values of $D_{Cu}$ are semi-quantitative. For each sample, the two values derived independently are in reasonable agreement. The observed interface drift can thus be interpreted as the classical Kirkendall effect. The values of $\tilde{D}$, $U$ and $\partial X_{Cu}/\partial x$ are not accurate

**Table 2**
Values of $D_{Cu}$ at 673 K and anneal time of 23 min.

| | $D_{Cu}$ ($m^2$ $s^{-1}$) 56Cu multilayer | 59Cu multilayer |
|---|---|---|
| from $\tilde{D}$, Eq. (2) | $2.7 \times 10^{-19}$ | $5.9 \times 10^{-19}$ |
| from $U$, Eq. (3) | $1.7 \times 10^{-19}$ | $6.4 \times 10^{-19}$ |

enough to permit the complete analysis to evaluate $D_{Zr}$, but we can conclude from the similarity of the independently derived values of $D_{Cu}$ that $D_{Zr}$ is negligible compared to $D_{Cu}$ at 673 K. As seen for $\tilde{D}$, the values of $D_{Cu}$ also are (2–3) × higher at 59Cu than at 56Cu.

### 3.5. Kirkendall voiding

An as-deposited sample of 56Cu was heated in-situ in TEM to ~718 K (thermal profile in Fig. S1). As $T_g$ for 56Cu is 687 K, this 'flash' heating takes the sample well into the supercooled liquid state. The time above $T_g$ was short to avoid any crystallization (studied in Cu-Zr thin films [25]). The flash-heating causes thinning of the Cu-rich layers, thickening of the Zr-rich layers and the development of inhomogeneity in the Cu-rich layers (Fig. 5). The extent of layer-thickness change is (by interpolation of the data in Fig. 4b) equivalent to the effect of annealing at 673 K for 27 min).

Autocorrelation analysis of HRTEM images [26] of the as-deposited and flash-heated samples (Fig. 6a,b) characterizes local atomic configurations across the whole image. The maps in Fig. 6c,d show the local autocorrelation function for a range of scattering vector $q$ (Fig. S2), and are sensitive to local changes in average atomic distance. The contrast between the Cu-rich and Zr-rich layers is evident in the as-deposited sample (Fig. 6c) but barely detectable after flash-heating (Fig. 6d). Within the Cu-rich layer after flash-heating, the autocorrelation pattern shows no correlation with the pattern of lighter and darker areas in the bright-field image (Fig. 6b), ruling out any inhomogeneity in composition or structure associated with these areas. We conclude that the observed features are nanovoids. These Kirkendall voids form in the Cu-rich layers because of diffusional asymmetry. The voiding

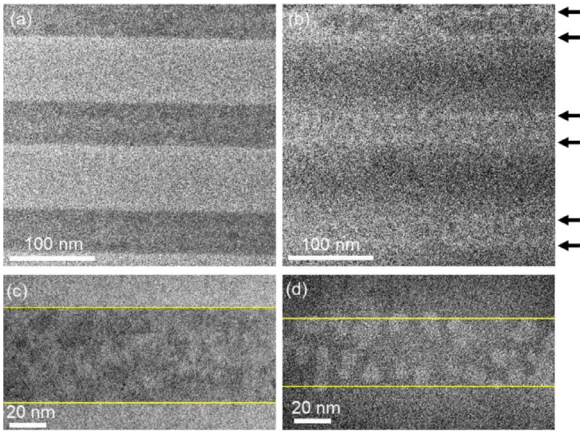


**Fig. 5.** A cross-sectional thin foil of the 56Cu multilayer: (a,c) as-deposited and (b,d) after *in-situ* flash-heating (Fig. S1). These bright-field images in TEM (a,b) and HRTEM (c,d) show a reversal in contrast from the as-deposited multilayer in which the Cu-rich layers are darker, to the flash-heated sample in which the Zr-rich layers are darker. As explained in the text, this reversal is attributed to the development of thickness variation in the thin foil, driven by the Kirkendall effect in which interdiffusion gives a net transport of volume out of the Cu-rich layers (Fig. S3). The arrows in (b) show the positions of most intense voiding. The lines in (c,d) are guides to the eye, indicating the interfaces between a Cu-rich layer and its Zr-rich neighbours.

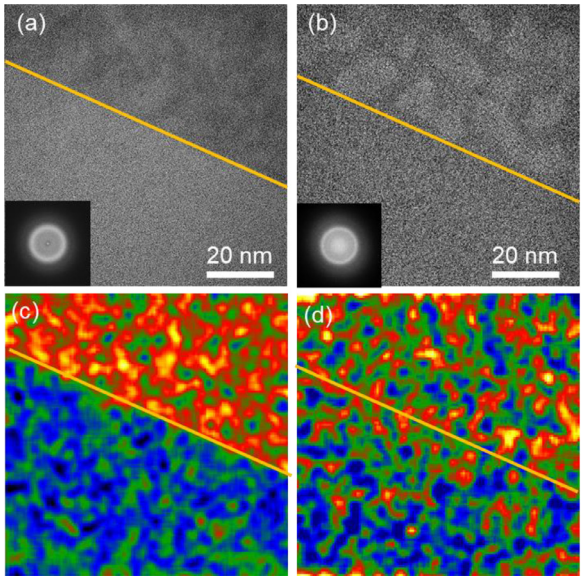


**Fig. 6.** An interface between Cu-rich and Zr-rich layers in a 56Cu sample showing the effect of in-situ flash heating into the supercooled liquid state. HRTEM images, with Cu-rich layer at top and Zr-rich layer at bottom, for (a) the as-deposited sample, (b) after *in-situ* flash heating (Fig. S1) up to 718 K. The insets are fast Fourier transforms of the whole images showing that the structures are fully amorphous. Autocorrelation analysis (Fig. S2) of the HRTEM images for (c) the as-deposited sample, (d) after *in-situ* flash heating. This analysis of the flash-heated sample suggests no inhomogeneity in structure or composition in the Cu-rich layer; accordingly, the contrast seen in the HRTEM image (b) is attributed to nanovoids.

is most evident adjacent to the interfaces with the Zr-rich layers (arrowed in Fig. 5b), as expected according to conventional studies of Kirkendall effects [24], and it occurs on annealing at higher temperature, where the rate of diffusive transport is more likely to overwhelm the strain accommodation mechanisms [27].

The diffusional asymmetry in the Cu-Zr amorphous phase transports volume from the Cu-rich to the Zr-rich layers (§3.4). Initially this leads to thinning of the Cu-rich layers. Later, if voids form in the Cu-rich layers, it is expected that, largely, the thinning stops and further reduction in the copper content in these layers is accommodated by the voiding. From the measured thinning, we estimate the composition of the Cu-rich and Zr-rich layers at the onset of voiding to be $Cu_{67}Zr_{33}$ and $Cu_{50}Zr_{50}$.

In the absence of EDX measurements, we use shifts in the first peak $q_1$ in $S(q)$ to consider changes in the composition of the layers (Supplementary Material §S.1). In the flash-heated 56Cu multilayer, the layer compositions are estimated to be $Cu_{66}Zr_{34}$ and $Cu_{51}Zr_{49}$. These are, within error, the same as those estimated from the layer thinning. We infer that the voids develop only in later stages of the interdiffusion enabled by the flash-heating.

In bright-field TEM images of the multilayer cross-sections, assuming uniform thickness of the thin foil, areas with greater density appear darker (evident for the Cu-rich layers in the as-deposited multilayer, Fig. 5a). This contrast is reversed relative to that in dark-field images, Fig. 1a,c. Annealing induces decay of the composition modulation and, when a uniform-thickness thin foil is subsequently prepared, the resultant contrast between the layers is reduced (Figs. 1b,d). When the thin foil is prepared first and then annealed (as in the in-situ flash-heating), a different effect is observed: the contrast does not decay, but reverses (Fig. 5a,b), the Zr-rich layers becoming darker. In the former case, the volume transport arising from the asymmetric diffusion is accommodated by normal strains perpendicular to the substrate; there can be no dimensional changes in the plane parallel to the substrate. In the latter case, the thickness of the Cu-rich layers in the multilayer

stack and the thickness of the thin-foil cross-section prepared from that stack are both ~50 nm. Thus the volume transport on flash-heating can be accommodated by changing the thickness of the thin foil.

On annealing, the Zr-rich layers swell (increasing the thickness through which the electron beam must travel) and the Cu-rich layers shrink. Such shape changes are expected when the thin-foil thickness is comparable to the diffusion distance $2\sqrt{\tilde{D}t}$ [28]. The effect of the thickness variation outweighs the effect of density difference, leading to the reversal of the contrast. The thickness modulation that develops in the thin foil (Fig. S3) complicates the analysis of interdiffusion kinetics, and precludes direct comparison with the results of annealing before thin-foil preparation, but it directly validates the concept of volume transport from the Cu-rich to the Zr-rich layers. The development of voids must expand the overall volume of the multilayer and, if all strains were normal to the substrate, that would lead to an increase in $\Lambda$. Such an increase is not observed, presumably because of the accommodation of volume transport by variations in the thin-foil thickness.

Voiding in the central Ni-rich layer of an annealed amorphous trilayer of Ni-Zr [29] was seen only at high temperature, attributed to the onset of diffusion of the slower species (Zr) and considered to represent an "opposite" Kirkendall effect [29,30]. The diffusional asymmetry in the amorphous Cu-Zr and Ni-Zr systems is expected to be similar. In the present work, the phenomena of interface drift and of voiding at higher temperature (and in the expected location) fit the classical Kirkendall effect, with no evidence for any "opposite" behaviour. We attribute the onset of voiding in the earlier study [29] simply to more rapid transport of volume at higher temperature.

## 4. Discussion

### 4.1. Absolute values of $\tilde{D}$

In Supplementary Material (§S.2), we show that the $\tilde{D}$ values in the present work are consistent with earlier measurements (at generally lower $T/T_g$) in multilayers of amorphous LTM-ETM alloys in general, and Ni-Zr in particular. In multilayers, when $\Lambda$ is short, the interdiffusion kinetics can be in the Nernst-Planck, rather than the Darken, regime [9]. The $\Lambda$ in the present work is, however, roughly one order of magnitude longer than value expected to divide the two regimes [9]. This justifies the assumption, in §3.4, that the Darken analysis of interdiffusion is applicable. Correction for gradient-energy effects [21] is not necessary for the relatively long $\Lambda$ in the present work.

The viscosity $\eta$ and atomic or molecular diffusivity $D$ in liquids are linked through the Stokes-Einstein equation:

$$D = \frac{kT}{6\pi r\eta} \tag{4}$$

where $r$ is a radius characteristic of the diffusing species. In high-temperature pure metal liquids, Eq. (4) holds, within a factor of two, if $r$ is taken to be the Goldschmidt ionic radius of the element [22]. Taking these values for copper and zirconium (96 pm for $Cu^+$ and 87 pm for $Zr^{4+}$), and taking $\eta = 10^{12}$ Pa s at $T_g$, we apply Eq. (4) to estimate $D$ in amorphous Cu-Zr at $T_g$. With this approach, similar values are obtained for 56Cu and 59Cu and for copper and zirconium; they are all in the range $D$ = (5.2 to 6.6) × $10^{-24}$ $m^2$ $s^{-1}$. These predictions of $D$ can be compared with the values of $D^*_{Cu}$ from the measured $\tilde{D}$ for 56Cu and 59Cu, using Eq. (2) and the thermodynamic factor ($\Phi$ = 6.7 for Cu-Zr, §S.2). The activation energy of 131 kJ $mol^{-1}$ (as in §2.2 and §S.4) is used for the extrapolation from 673 K to the $T_g$ values for 56Cu and 59Cu. We obtain $D^*_{Cu}$ values of 6.7 × $10^{-20}$ $m^2$ $s^{-1}$ for 56Cu and 2.7 × $10^{-19}$ $m^2$ $s^{-1}$ for 59Cu, more than four orders higher than those predicted using Eq. (4). Thus the diffusion of copper in amorphous Cu-Zr is decoupled from viscous flow, not only well below $T_g$ but at $T_g$ itself. This is consistent with molecular-dynamics simulations of liquid $Cu_{65}Zr_{35}$ showing that the decoupling of atomic diffusion from viscous flow increases sharply as the temperature is lowered below ~$2T_g$ [31]. This decoupling permits the large diffusional asymmetry.

Estimated $D^*_{Zr}$ values at $T_g$ from the published data on other amorphous LTM-ETM alloys (§S.2) are in the range 2 × $10^{-24}$ $m^2$ $s^{-1}$ to 1 × $10^{-21}$ $m^2$ $s^{-1}$ and therefore possibly not so far decoupled from the value expected from the viscosity and Eq. (4).

### 4.2. Composition dependence of $D_{Cu}$

The measured $\tilde{D}$ at 673 K is higher at 59Cu than at 56 Cu, and the difference in values (a factor of 2–3 ×) is large, given the small composition difference. Considering possible effects of composition (§S.3), we conclude that $D_{Cu}$ must itself be strongly dependent on the composition of the amorphous alloy. The Cu-Zr amorphous system has been well studied over the accessible composition range. Its structure has been related to its atomic packing density, glass-forming ability (GFA) and mechanical properties. The ratio of the atomic radii of copper and zirconium is such that the first coordination shell of atom-centred clusters is efficiently packed [32]. This allows the amorphous phase to be densely packed, and there is interest in the composition dependence of the packing density [11,33]. In the absence of other factors, the higher the packing density, the lower the critical cooling rate for glass formation [11]. It is presumed, but not yet directly demonstrated, that this also lowers the atomic mobility in the liquid and glassy states.

The amorphous phase is taken to be more densely packed if $\Delta V/V$, its excess volume over that of the crystalline state at the same composition, is less. Atomistic molecular-dynamics simulations suggest that, over the composition range of present interest, $\Delta V/V$ decreases monotonically with increasing copper content [33]. The directly measured $\Delta V/V$ shows more complex behaviour, with local minima indicating 'unexpectedly and unexplainably sharp' peaks in packing density (Fig. 7a) [11]. The minima in $\Delta V/V$ show an excellent correlation with higher values of the critical plate thickness that can be cast fully glassy (Fig. 7b) [11]. The composition 56Cu lies near a minimum in $\Delta V/V$ and a maximum in critical thickness of ~1.0 mm. In contrast, for 59Cu, the critical thickness is ~0.7 mm, which for Newtonian cooling implies a critical cooling rate that is over 40% higher.

The correlation between $\Delta V/V$ and critical thickness (Fig. 7) can now be extended to include atomic diffusivities, which are also found to show a sharp composition dependence. At 673 K, in 59Cu the values of $\tilde{D}$ and $D_{Cu}$ are (2–3) × higher than in 56Cu, while $D_{Zr}$ is expected to be (3–5) × lower. This suggests that greater interdiffusivity ($\propto D_{Cu}$) and greater decoupling of $D_{Cu}$ and $D_{Zr}$, are linked to less dense packing and lower GFA. The fragility $m$ of liquid Cu-Zr has been estimated at several compositions [34], but unfortunately with composition resolution insufficient to determine whether or not $m$ shows sharp variations consistent with Fig. 7 and with the present work. In the absence of any prior reports of the composition dependence of atomic diffusivities in amorphous Cu-Zr, the present work provides the first evidence for the effect of atomic packing density on interdiffusivity.

We speculate that in the 56Cu amorphous alloy, a high proportion of the copper atoms are in stable, atom-centred clusters (often icosahedral [33]). In comparison, 59Cu has excess copper atoms that are not in such clusters; the packing is then less dense overall, and the excess copper atoms are more mobile, contributing to a higher interdiffusivity that is more decoupled from $D_{Zr}$ and from viscous flow.

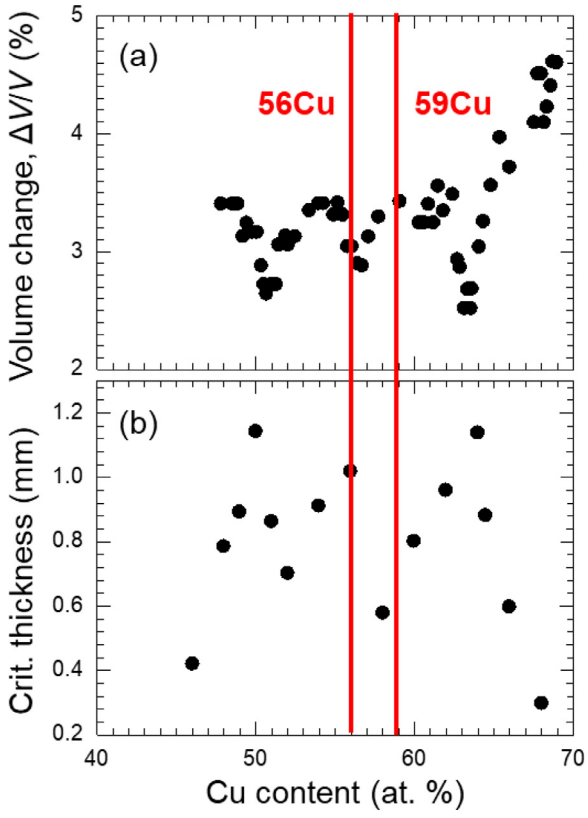


**Fig. 7.** Property variation with composition reported for amorphous Cu-Zr. (a) Excess volume of the amorphous alloy (relative to the crystalline state) measured in cantilever samples [11]. (b) The upper limit on plate thickness that can be cast fully glassy [11]. The vertical lines show the compositions 56Cu and 59Cu in the present work. Data from [11] used with permission from the American Association for the Advancement of Science.

### 4.3. Kirkendall voiding in the liquid

As discussed in §S.4, the speed of the changes in the in-situ flash-heating of 56Cu show that the sample has entered the supercooled liquid state. In high-temperature metallic alloy liquids, the diffusivities of small and large atomic species are similar, but they diverge on cooling in the liquid and into the glassy state, with smaller species being faster [3]. The asymmetry of diffusion in amorphous LTM-ETM systems can be extreme: in amorphous $Ni_{55}Zr_{45}$ multilayers annealed at $T = 0.62\ T_g$, $(D^*_{Ni}/D^*_{Zr}) \approx 6 \times 10^4$ [9]. As a fraction of $T_g$, the maximum (~718 K) reached in the present in-situ annealing of 56Cu (§3.5) would scale to 684.5 K in $Ni_{55}Zr_{45}$; taking the earlier data [9] and extrapolating to 684.5 K, we estimate that $(D^*_{Ni}/D^*_{Zr}) \approx 74$. Taking conventionally determined tracer diffusivities [2], an even higher value of $(D^*_{Ni}/D^*_{Zr})$ would be obtained.

Assuming similar behaviour in amorphous Cu-Zr in the present case, and despite the novelty of making measurements in the liquid state, significant diffusional asymmetry ($D_{Cu} \gg D_{Zr}$) is expected, leading to strong Kirkendall effects. Darken's analysis of interdiffusion [23] is independent of atomistic mechanisms of diffusion, but in crystalline systems it is common to consider interface drift and voiding in terms of the diffusion of vacancies. The present observation of Kirkendall voiding in the liquid definitively rules out the formation of voids by condensation of vacancies. The voids are formed in thin foils, in which any triaxial tensile stresses in the Cu-rich layers must be low. It is interesting, then, that the collapse of free volume leads to voiding rather than overall shrinkage. This may reflect the diffusional asymmetry in which the high mobility of copper promotes volume transport, while the low mobility of zirconium inhibits viscous flow.

Diffusional asymmetry in LTM-ETM systems has been linked to *solid-state amorphization* in which two polycrystalline elements (e.g. nickel and zirconium), when in contact, form an amorphous reaction interlayer on annealing. Roughly, the fast nickel permits diffusional mixing, while the slow zirconium inhibits the nucleation and growth of equilibrium crystalline intermetallic compounds [2]. In the present case, such an asymmetry ($D_{Cu} \gg D_{Zr}$) extends into the liquid state, and we speculate that this facilitates the characterization of interdiffusion before any onset of crystallization upon annealing. The diffusional asymmetry may also be related to the GFA of this system.

### 4.4. TEM techniques for characterizing atomic diffusion

While TEM-based determination of composition profiles is useful to characterize interdiffusion in metastable systems (§S.5), it has limitations. The evolving composition profile is of particular interest for systems with asymmetric interdiffusion, yet in the present measurements, the diffusivity of copper is so dominant that it is not possible to extract any values for the diffusivity of zirconium. Thin foils must be prepared after each anneal, and thus it is cumbersome to collect data to allow fine resolution of time-dependent behaviour. It may not be possible to apply in-situ heating to circumvent this problem; we show that in the present system, thickness relaxation of the thin foil leads to behaviour particular to that geometry and not characteristic of the bulk system.

## 5. Conclusions

Multilayered (compositionally modulated) samples of amorphous Cu-Zr are sputter-deposited and annealed. Cross-sectional thin foils prepared from these samples are characterized by EDX in TEM. The evolution of the composition profiles on annealing gives the interdiffusivity $\tilde{D}$. There have been many studies (using other methods) of atomic diffusion in the related amorphous systems (Co,Fe,Ni)-Zr, but not in Cu-Zr itself. The $\tilde{D}$ in Cu-Zr is broadly consistent with extrapolations from the earlier measurements compared at the same reduced temperature ($T/T_g$). The present values of $\tilde{D}$ are obtained for $(T/T_g) = 0.95$ to 0.98, a higher reduced temperature than in most earlier work. The EDX profiling quantifies the Kirkendall drift of the multilayer interfaces and the local composition gradients. The measured drift velocities at 673 K are 2 to 4 pm $s^{-1}$. The Darken analysis of interdiffusion kinetics ($\tilde{D}$ and drift velocity) is applied, taking into account that the atomic volume of zirconium is twice that of copper. In the present measurements, the diffusivity of copper is so dominant that it is not possible to extract values for the diffusivity of zirconium.

The interdiffusivities at 673 K are $1.7 \times 10^{-19}$ $m^2$ $s^{-1}$ for amorphous $Cu_{56}Zr_{44}$, and $3.4 \times 10^{-19}$ $m^2$ $s^{-1}$ for $Cu_{59}Zr_{41}$. Extrapolating to $T_g$, these values are more than four orders of magnitude higher than would be predicted from the viscosity via the Stokes-Einstein equation; this decoupling of atomic diffusion from viscous flow permits strong diffusional asymmetry even at $T_g$. That $\tilde{D}$ is so different at the similar compositions 56Cu and 59Cu correlates well with a local maximum in atomic packing fraction and local maximum in glass-forming ability near 56Cu. The measurements of $\tilde{D}$ provide the first direct confirmation that interdiffusivity in the amorphous state is lower at higher packing density. We suggest that at 56Cu, most copper atoms are in stable, atom-centred clusters with efficient packing in the first-neighbour shell, and that at 59Cu, copper atoms not in such clusters contribute to the faster transport, and to greater decoupling of $D_{Cu}$ from $D_{Zr}$ and from viscous flow.

EDX characterization of composition profiles can yield quantitative estimates of interdiffusivity. The multilayer geometry allows Kirkendall drift to be measured without the need for embedded inert markers. The composition profiles in amorphous Cu-Zr retain some square-wave character even after substantial homogenization. The ability to detect such effects of non-Fickian diffusion is an important advantage of this novel TEM method.

In-situ flash heating of a multilayer of overall composition 56Cu in the TEM shows interdiffusion, interface drift, and ultimately the formation of Kirkendall nanovoids in the Cu-rich layers. This is expected given that $D_{Cu} \gg D_{Zr}$, but it is novel that the voiding occurs in the supercooled liquid. The voiding cannot be attributed to the condensation of vacancies, but to a general volume transport, further verified by the development of a thickness modulation in the in-situ annealed TEM thin foil. The diffusional asymmetry in the liquid state may influence the resistance to crystallization and the glass-forming ability.

## Declaration of Competing Interest

The authors declare that they have no known competing financial interests or personal relationships that could have appeared to influence the work reported in this paper.

## Acknowledgments

We acknowledge access to the facilities in the electron Physical Science Imaging Centre (ePSIC) at the Diamond Light Source, and thank M. Danaie for technical support of the data acquisition during the in-situ heating HRTEM experiments (Proposal No. MG24245). We thank D.V. Louzguine-Luzgin, A. Rodin and D. Şopu for useful discussions, and C. Mitterer and V. Terziyska for providing access to the sputtering device and for advice on thin-film deposition. We are grateful to the anonymous reviewer for helpful comments. We acknowledge support from the European Research Council: for A.L.G. and Y.P.I. under the Advanced Grant "ExtendGlass – Extending the range of the glassy state: Exploring structure and property limits in metallic glasses" (grant ERC-2015-AdG-695487); and for J.E., S.V.K. and B.P. under the Advanced Grant "INTELHYB – Next generation of complex metallic materials in intelligent hybrid structures" (grant ERC-2013-ADG-340025). J.E. also acknowledges support from the Ministry of Science and Higher Education of the Russian Federation in the framework of the Increase Competitiveness Program of MISiS (Support project for young research engineers, project no. K2–2020–046). Z.Z. acknowledges support from the China Scholarship Council.

## Supplementary materials

Supplementary material associated with this article can be found, in the online version, at doi:10.1016/j.actamat.2021.116993.

## References

[1] H. Hahn, R.S. Averback, S.J. Rothman, Diffusivities of Ni, Zr, Au, and Cu in amorphous Ni-Zr alloys, Phys. Rev. B 33 (1986) 8825–8828.
[2] A.L. Greer, N. Karpe, J. Bøttiger, Diffusional aspects of the solid state amorphizing reaction, J. Alloys Compd. 194 (1993) 199–211.
[3] F. Faupel, W. Frank, M.P. Macht, H. Mehrer, V. Naundorf, K. Rätzke, H.R. Schober, S.K. Sharma, H. Teichler, Diffusion in metallic glasses and supercooled melts, Rev. Mod. Phys. 75 (2003) 237–280.
[4] D. Turnbull, Amorphous solid formation and interstitial solution behavior in metallic alloy systems, J. Phys. Coll. 35 (1974) C4.1–4.10.
[5] F. Delogu, Atomistic mechanism of the formation of a nanometer-sized amorphous metal by Kirkendall effect, Mater. Chem. Phys. 125 (2011) 390–396.
[6] Y. Zhao, J. Liu, C. Liu, F. Wang, Y. Song, Amorphous CuPt alloy nanotubes induced by $Na_2S_2O_3$ as efficient catalysts for the methanol oxidation reaction, ACS Catal. 6 (2016) 4127–4134.
[7] A.-A. El Mel, R. Nakamura, C. Bittencourt, The Kirkendall effect and nanoscience: hollow nanospheres and nanotubes, Beilstein J. Nanotechnol. 6 (2015) 1348–1361.
[8] J.S. Conyers, M.J. Hall, A.L. Greer, R.E. Somekh, The effect of diffusion-induced stress on the magnetic properties of c-Ni/a-$Ni_{50}Zr_{50}$ multilayers, J. Magn. Magn. Mater. 156 (1996) 419–420.
[9] A.L. Greer, Stress effects on interdiffusion in amorphous multilayers, Defect Diffus. Forum 129–130 (1996) 163–180.
[10] F.L. Yang, R.E. Somekh, W.C. Shih, A.L. Greer, Measurements and simulation of asymmetric interdiffusion in amorphous Ni-Zr multilayers, Mater. Sci. Forum 179–181 (1995) 807–812.
[11] Y. Li, Q. Guo, J.A. Kalb, C.V. Thompson, Matching glass-forming ability with the density of the amorphous phase, Science 322 (2008) 1816–1819.
[12] Zs. Czigány, G. Radnóczi, K. Järrendahl, J.E. Sundgren, Annealing induced interdiffusion and crystallization in sputtered amorphous Si/Ge multilayers, J. Mater. Res. 12 (1997) 2255–2261.
[13] F. Güder, Y. Yang, S. Goetze, A. Berger, R. Scholz, D. Hiller, D. Hesse, M. Zacharias, Toward discrete multilayered composite structures: do hollow networks form in a polycrystalline infinite nanoplane by the Kirkendall effect? Chem. Mater. 23 (2011) 4445–4451.
[14] N. Mattern, A. Schöps, U. Kühn, J. Acker, O. Khvostikova, J. Eckert, Structural behavior of $Cu_xZr_{100-x}$ metallic glass (x = 35–70), J. Non Cryst. Solids 354 (2008) 1054–1060.
[15] Yu.P. Ivanov, C.M. Meylan, N.T. Panagiotopoulos, K. Georgarakis, A.L. Greer, *In-situ* TEM study of the crystallization sequence in a gold-based metallic glass, Acta Mater. 196 (2020) 52–60.
[16] D.V. Louzguine-Luzgin, C.L. Chen, L.Y. Lin, Z.C. Wang, S.V. Ketov, M.J. Miyama, A.S. Trifonov, A.V. Lubenchenko, Y. Ikuhara, Bulk metallic glassy surface native oxide: its atomic structure and electrical properties, Acta Mater. 97 (2015) 282–290.
[17] A.Z. Moshfegh, O. Akhavan, A calculation of diffusion parameters for Cu/Ta and Ta/Si interfaces in Cu/Ta/Si(1 1 1) structure, Mater. Sci. Semicond. Process. 6 (2003) 165–170.
[18] J. DuMond, J.P. Youtz, An X-ray method of determining rates of diffusion in the solid state, J. Appl. Phys. 11 (1940) 357–365.
[19] A.L. Greer, Interdiffusion in amorphous multilayered materials, Annu. Rev. Mater. Sci. 17 (1987) 219–233.
[20] A.L. Greer, Measurements of atomic diffusion using metallic multilayers, Curr. Opin. Solid State Mater. Sci. 2 (1997) 300–304.
[21] F.L. Yang, A.L. Greer, R.E. Somekh, Effects of short-range ordering on interdiffusion in Ag/Au epitaxial multilayers, Thin Solid Films 275 (1996) 258–261.
[22] A.L. Greer, Atomic transport and structural relaxation in metallic glasses, J. Non Cryst. Solids 61&62 (1984) 737–748.
[23] L.S. Darken, Diffusion, mobility and their interrelation through free energy in binary metallic systems, Trans. AIME 175 (1948) 184–201.
[24] A. Paul, T. Laurila, V. Vuorinen, S.V. Divinski, Thermodynamics, Diffusion and the Kirkendall Effect in Solids, Springer, Cham, 2014.
[25] D. Lee, J.J. Vlassak, Diffusion kinetics in binary CuZr and NiZr alloys in the super-cooled liquid and glass states studied by nanocalorimetry, Scr. Mater. 165 (2019) 73–77.
[26] B. Sarac, Yu.P. Ivanov, A. Chuvilin, T. Schöberl, M. Stoica, Z.L. Zhang, J. Eckert, Origin of large plasticity in Fe-based bulk metallic glasses, Nat. Commun. 9 (2018) 1333.
[27] S. Cogan, S. Kwon, J. Klein, R. Rose, Fabrication of large diameter external-diffusion processed $Nb_3Sn$ composites, IEEE Trans. Magn. 19 (1983) 1139–1142.
[28] W.J. Boettinger, G.B. McFadden, S.R. Coriell, R.F. Sekerka, J.A. Warren, Lateral deformation of diffusion couples, Acta Mater. 53 (2005) 1995–2008.
[29] K.N. Tu, T.C. Chou, Submicron void formation in amorphous NiZr alloys, Phys. Rev. Lett. 61 (1988) 1863–1866.
[30] P. Klugkist, K. Rätzke, F. Faupel, Evidence of defect-mediated zirconium self-diffusion in amorphous $Co_{92}Zr_8$, Phys. Rev. Lett. 81 (1998) 614–617.
[31] Q.L. Cao, P.P. Wang, D.H. Huang, Revisiting the Stokes–Einstein relation for glass-forming melts, Phys. Chem. Chem. Phys. 22 (2020) 2557–2565.
[32] D.B. Miracle, W.S. Sanders, O.N. Senkov, The influence of efficient atomic packing on the constitution of metallic glasses, Philos. Mag. 83 (2003) 2409–2428.
[33] K.W. Park, J.I. Jang, M. Wakeda, Y. Shibutani, J.C. Lee, Atomic packing density and its influence on the properties of Cu–Zr amorphous alloys, Scr. Mater. 57 (2007) 805–808.
[34] K. Russew, L. Stojanova, S. Yankova, E. Fazakas, L.K. Varga, Thermal behavior and melt fragility number of $Cu_{100-x}Zr_x$ glassy alloys in terms of crystallization and viscous flow, J. Phys. Conf. Ser. 144 (2009) 012094.